NUMERICAL PREDICTION OF TRACTIVE PERFORMANCE OF TRACK-SOIL INTERACTION SYSTEM THROUGH DIFFERENT GROUSER HEIGHTS

Ge Jun[1], Shuai Peng[1], Chengmao Cao[1], Liangfei Fang[1], Kuan Qin[1*]

[1*]Corresponding author. School of Engineering, Anhui Agricultural University, Hefei, 230036, China.
Email: qinkuan@ahau.edu.cn | ORCID ID: https://orcid.org/0000-0002-4411-9631

ABSTRACT

This study aims to investigate the influence of moisture contents and grouser heights on traction force exerted on different surfaces in the track-soil interaction system. A sandy loam was employed for acquiring the soil parameters, such as kc, $k\varphi$, n, C, Ca, δ, φ, and γ. These parameters were obtained through the mean of the bevameter technique. Moisture contents of the sandy loam were changed from low to high levels, which could be listed as 1.4%, 8.0%, 14.7%, and 22.2% at last. The direct shear and penetration tests were performed for each soil condition of the moisture content, respectively. The model of the single-grouser-shoe (track model) had a length of 9 cm, a width of 15 cm, and varied grouser heights from 0 to 15 cm with a 0.5 cm interval. Based on the calculation result, in general, the shearing force produced by the bottom surface always performs better than either the shear force on the grouser-tip surface or two lateral surfaces. Simultaneously, prediction results also show that the shearing forces were significantly influenced by the level of moisture content in the soil.

INTRODUCTION

Due to the simple sliding steering of the tracked vehicles and excellent tractive performance in varied ground conditions (Wang et al., 2018; Guo et al., 2019), the apron wheel is widely equipped in agricultural and armoured vehicles and mobile robots (Yuta, 2017; Mocera & Nicolini, 2018; Wong et al., 2018). To improve the track tractive performance, single grouser shoes are always equipped on tracked vehicles/rovers to achieve better performance on terrain trafficability (Amir Ali Forough Nassiraei & Skonieczny, 2020). Relevant studies showed that the traction force generated by a track is through the process of terrain/soil shearing, and the tractive performance of the track-laying-vehicles is determined by the interaction between the track and the soil, which strongly depends on the structure of the track, such as the track of shoes and belt, and the soil of moisture content (Gill & Vanden Berg, 1967; Yokoyama et al., 2020). As an essential issue in the terramechanics, the prediction of tractive performance is extensively concerned by researchers (Battiatoetal & Diserens, 2017; Feng et al., 2018; ten Damme et al., 2021; Xu et al., 2022; Sandu et al., 2019). Furthermore, forces generated on different horizontal surfaces in a grouser shoe-soil interaction system are always considered a piece of significant information for promoting tractive performance through the method of parameter optimization (Ani et al., 2018; Edwin et al., 2018; Shin et al., 2020; Li et al., 2021; Zhou et al., 2021).

Bekker (1969) introduced the interaction relationship between a structure and a terrain condition in the book Introduction to terrain-vehicle systems. Some empirical formulas have been introduced for calculating or predicting the thrust, resistance, and traction forces of the running gear-terrain interaction system in that book. Bekker (1969) also proposed a modulus named the Cone Index (CI) to assess vehicle mobility on a "go/no go" basis, which focused on the capacity to support the ability of a terrain. In addition, the drawbar pull of tracked vehicles has absorbed significant attention from researchers for decades (Das, 1979; Ge et al., 2019). Yamada et al. (2021) tested an experimental track-laying vehicle on underwater ground and non-underwater ordinary ground, based on tracked vehicles, to study the fundamental principles of the dynamic interaction between the crawler of tracked vehicle and soil on underwater ground. That experiment measured the cone index of underwater

ground and non-underwater ordinary ground. In addition, the research also showed that the tractive efficiency of tracked vehicles on the underwater ground was lower than the ordinary ground (Yamada et al., 2021). To clear up the concept of thrust generation on soft ground with respect to the slip mentioned in Dr. Bekker's first book Theory of Land Locomotion (Bekker, 1956), Baek et al.（2018）assessed the off-road tracked vehicle's performance by evaluating both the bottom thrust and the side thrust based on the punching shear theory. Additionally, in that research, a prediction model for the side thrust was newly developed, and a series of model track experiments on a model track system with silty sand track experiments were conducted to assess the off-road tracked vehicle's performance. (Baek et al., 2018). Yang et al. (2018) reported a new calculation method for deducing pressure–sinkage of tracked vehicles in rough terrain considering moisture and sinkage speed and conducted a series of pressure–sinkage tests to analyse the effect of water content, sinkage speed, and number of loadings on three parameters of the Bekker's model (Yang et al., 2018).

It could be noticed that the research introduced above paid more attention to the aspect of the overall performance or the force generation by an entire track. Some of the other studies also extend the interest into the aspect of the shear force at a certain side or even into the reacting force with soil deformation by the single grouser shoe (Cutini et al., 2020). Such as, Zhang et al. (2022) reported soil bulk density and water content were the key factors influencing shear strength. That research found that the main influencing factors of cultivated layer shear strength for sloping farmland are bulk density and water content, and the shear strength of unsaturated soil is greatly affected by the change in water content (Zhang et al., 2022). Suzuki et al. (2019) examined the applicability of resistive force theory for the analysis of a traveling wheel with grouser by comparing it using the Discrete Element Method (DEM) analysis results. For this purpose, the researchers conducted plate intrusion/extrusion and a wheel traveling analysis for loose frictional soil as a virtual test based on the DEM (Suzuki et al., 2019). Ge et al. (2016b) performed research comparing the tractive performance of steel and rubber single grouser shoes under different soil moisture contents. According to the conclusions of that study, it could be known that the steel performed better than the rubber at drawbar pull generation with a single grouser shoe. Shaikh et al. (2021) performed research on the interaction of a single grouser shoe with clay loam terrain at varying moisture content using the discrete element approach. The research verified the feasibility of the EDM model again.

From what we introduced above, it can be seen that the side\lateral shear force in the track\grouser shoe-soil interaction system should be clarified and is a piece of significant information for the optimization study on promoting the tractive performance. Moreover, the results could also provide significant conclusions utilized for explaining the effect of the track or grouser shape on the drawbar pull generation.

MATERIAL AND METHODS

Hereinafter, a theoretical prediction method for calculating the shear force will be introduced. The materials and methods employed in this study are described as follows:

TABLE 1. Dimensions of the single grouser shoe.

Dimension of the grouser shoe	Representation	Value
Pitch, cm	L	9
Width, cm	B	15
Height, cm	t	3
Ratio of grouser thickness	λ	0.1
Height of grouser, cm	h	0-15

Model of soil and grouser shoe

The thrust force of a grouser shoe could be influenced significantly by soil conditions (Wong, 2008; 2010; Tiwari et al., 2010). For instance, Ge et al. (2016a) introduced that the thrust and running resistance could be notably influenced by changes in the soil adhesion strength. For another example, Lyasko (2010) presented research on the quantitative evaluation of the multi-pass effect on off-road vehicle tractive performance in different soils. The soil can be classified based on a triangle classification system given by USDA (Plackett, 1985), and one kind of sandy loam has been utilized as the test soil for this experiment. The test soil has been changed with four different moisture contents from low to high levels that could be listed as 1.4%, 8.0%, 14.7%, and 22.2% (dry basis, D. B.).

The single grouser shoe shown in Fig. 1 was utilized as the test track to contact with the test soil. The dimensions of the single grouser shoe have been listed in Table 1.

The shear model and the prediction formulas

The forces in the grouser shoe-soil interaction system were introduced comprehensively in the book *The Theory of Land Locomotion* (Bekker, 1956) and the book *Introduction to terrain-vehicle systems* (Bekker, 1969) through a series of calculation equations. The soil's reacting force to a penetrated plate could be expressed as [eq. (1)].

$$q = \left(\frac{k_c}{b} + k_\varphi\right) \times (Z_0)^n \qquad (1)$$

Where:

k_c was the cohesion modulus in Bekker`s equation;

k_φ was the friction modulus in Bekker`s equation;

Z_0 was the sinkage of single grouser shoe;

n was the exponent of sinkage,

b was the width of single grouser shoe.
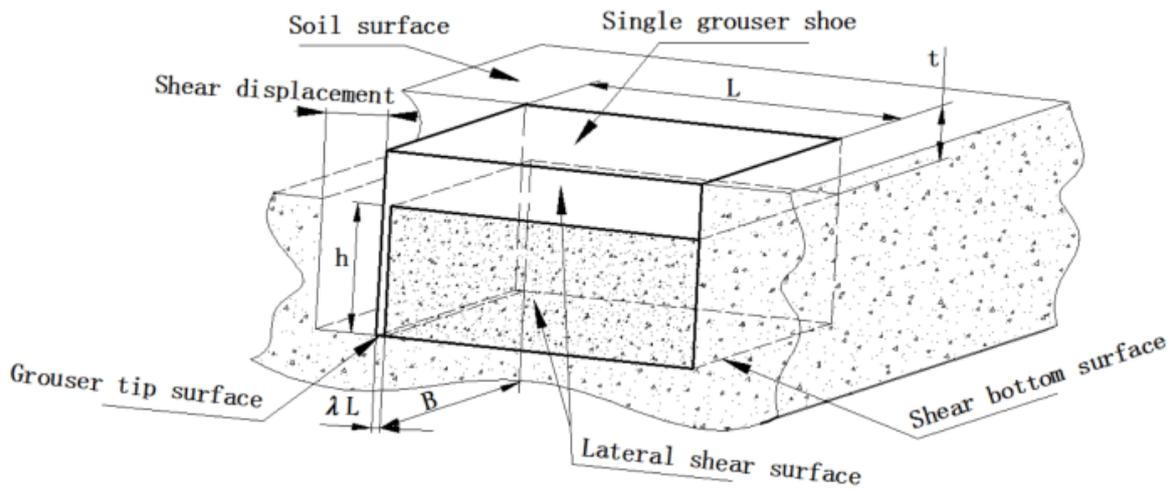
FIGURE 1. The single grouser shoe and the 3D direct shear model.
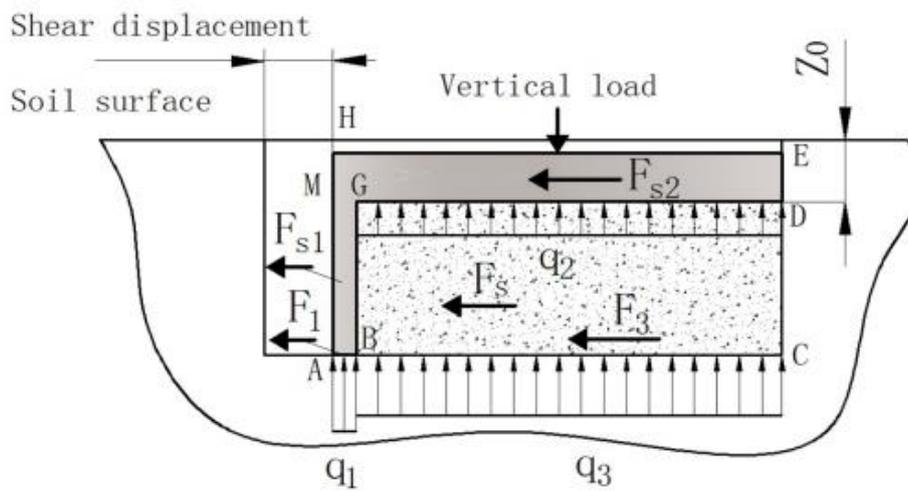
FIGURE 2. The forces acting on the track shoe when the soil shearing happens.

In this study, a 3D direct shear model was considered and the specific is has been shown in Fig. 1. Based on the figure, the grouser shoe pressed the soil down at first and then shear the soil around the shoe. In this process, the thrust force was generated by three failure or frictional surfaces: the two lateral failure\frictional surfaces and the bottom failure surface. Depending on Fig. 2, it could be further be understood clearly that the thrust consisted of the forces generated by the grouser tip surface, two lateral side surfaces, and the bottom surface, respectively.

Based on [eq. (1)] and the *Mohr-Coulomb* failure criterion, the force on grouser tip surface F_1 could be expressed as:

$$F_1 = \lambda LB \times (C_a + q_1 \times \tan \delta) \tag{2}$$

Here,

λ was the ratio of grouser thickness to the pitch of the grouser;

L was the length of the grouser shoe;

B was the width of the grouser shoe;

C_a was the soil adhesion strength;

q_1 was the soil's pressure on the grouser tip surface, and

δ is the external friction angle of soil to steel.

The force acting on the bottom surface F_3 could be described as:

$$F_3 = (1 - \lambda)LB \times (C + q_3 \times \tan \varphi) \tag{3}$$

Here,

C was the cohesion strength of the soil;

q_3 was the pressure on the bottom surface by the soil, and

φ was the internal friction angle of the soil.

According to Fig. 2, the lateral shear force comprises three parts: F_s, F_{s1}, and F_{s2}. The expression of mathematical prediction could be derived and was shown as follows:

$$F_s = (1 - \lambda)\{C + [q_2 + \gamma_t \times \frac{h + 2Z_0}{2}] \times \tan^2(45 - \frac{\varphi}{2}) \times$$
$$\tan \varphi - 2C \times \tan(45 - \frac{\varphi}{2}) \times \tan \varphi\} \tag{4}$$

Here,

q_2 was the pressure on the beneath surface of grouser spacing, and

γ_t was the bulk density of the test soil.

$$F_{s1} = \lambda hL\{C_a + tan\,\delta \times tan(45 - \frac{\varphi}{2})[\frac{\gamma_t\,(2Z_0 + h)}{2} \times$$

$$tan(45 - \frac{\varphi}{2}) - 2C]\} \qquad (5)$$

Where the h was the height of the grouser.

For the F_{s2}, the situation of $Z_0 > t$ was considered,

and the formula could be written as:

$$F_{s2} = \int_{Z_0-t}^{Z_0}(1 - \lambda)\,L\{C_a + [\gamma_t \times Z \times tan^2(45 - \frac{\varphi}{2}) -$$

$$2C \times tan\,\delta \times tan(45 - \frac{\varphi}{2})]\}dZ \qquad (6)$$

Here, the t was the height of the grouser spacing.

If the lateral shear force was denoted by F_2. It could be known that,

$$F_2 = 2(F_s + F_{s1} + F_{s2}) \qquad (7)$$

Experimental devices and instruments

Soil parameters that were utilized for predicting tractive performance could be investigated with the instrument so-called bevameter, and it mainly consisted of two parts: the penetration test device and the shear test device (Mason et al., 2020). In this study, the soil parameters of the sandy loam have been investigated by tests such as the direct shear test, the penetration test, the measurements of bulk density, and the moisture content.

The core part of the direct shear device was a shear box that could be separated into an upper box and a lower box. For different purposes, the upper box and the lower box could be put with different specimens like soil or circular steel plate. The diagrammatic illustration of the direct shear device is illustrated in Fig. 3. When a test was starting, the lower box was pushed forward by an electric motor. The moving distance of the lower box was detected by a displacement sensor. Meanwhile, the upper box was kept still by a rod connecting with a load cell. The test data has been recorded by a strainmeter and processed by a computer.
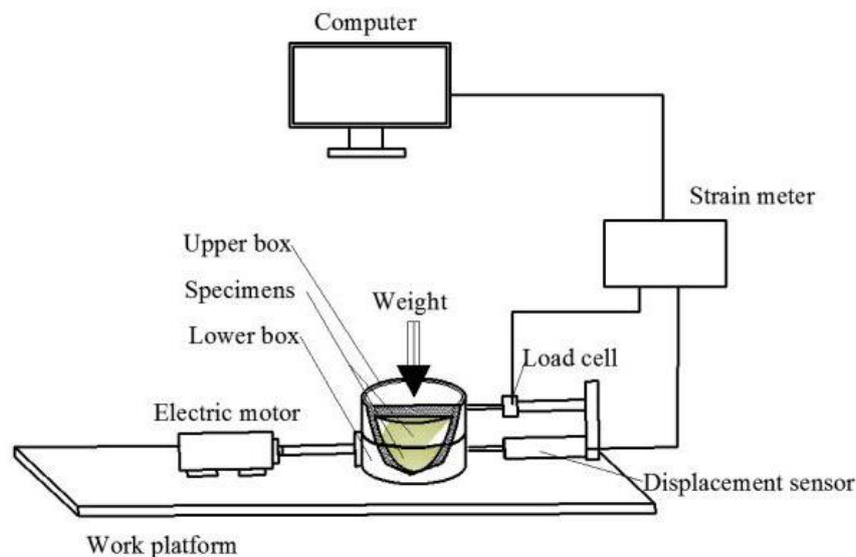
FIGURE 3. Diagrammatic illustration of the direct shear device.

The frictional modulus k_φ, the cohesive modulus k_c, and the sinkage exponent n could be acquired through the soil penetration test. As illustrated in Fig. 5, the penetration test device mainly consisted of the drive power, test plates, soil bin, sensors, data recording, and the processing part. If a penetration test was started, a test plate was going to be penetrated into the soil with a long rod driven by an electric motor. Details about the penetration depth and the soil's reaction force have been detected by the displacement transducer and the load cell, respectively. The test data also has been processed through the strainmeter and the computer.
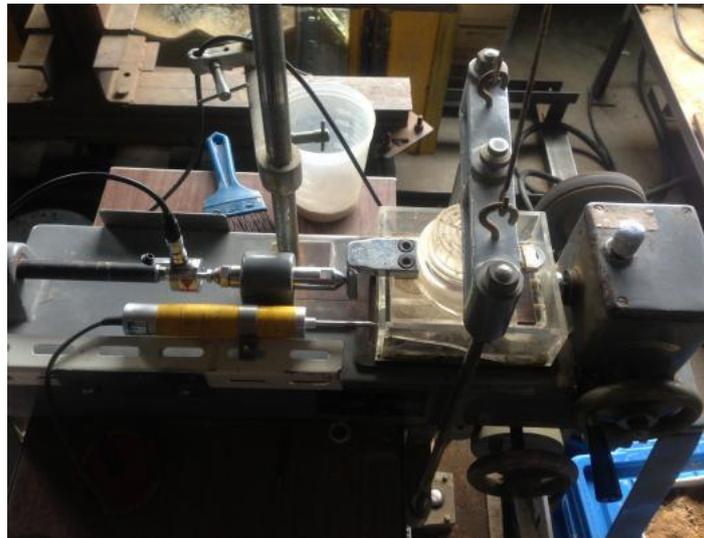
FIGURE 4. Locale photo of the direct shear device.
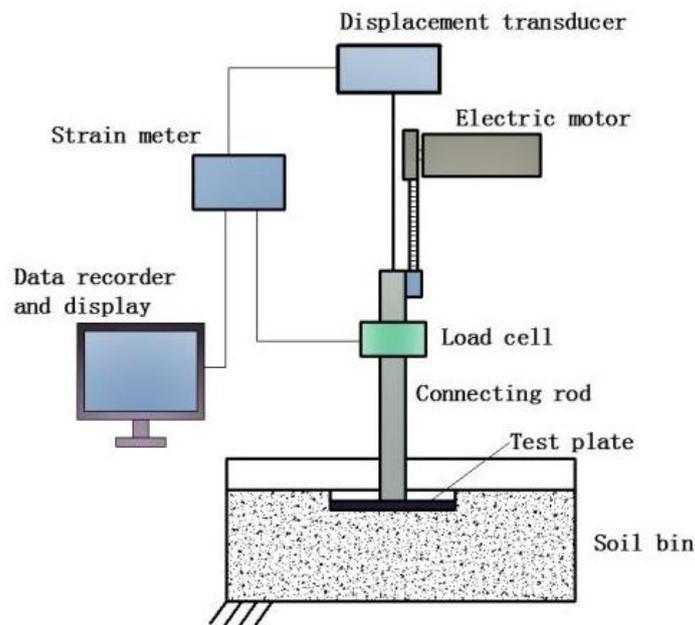
FIGURE 5. Diagrammatic illustration of the penetration device.

RESULTS AND DISCUSSION

Prediction for the thrust force of the single grouser shoe depended on the parameters of soil and the empirical formulas. In this study, the 3D direct shear model has been used for the shearing force prediction, and the experimental results were introduced as follows.

Soil parameters

Generally speaking, the saturation of sandy loam happens around the moisture content level at 30% (dry basis). Therefore, the test soil has been changed to four different levels of moisture content for investigating the concerned soil parameters under extreme dry, relatively low moisture content, normal moisture content, and high moisture content soil conditions. Specifically, the experiment classified soil moisture content into four different levels: 1.4% moisture content represents extremely dry sandy soil, 8.0% represents relatively low moisture content sandy soil, 14.7% represents normal moisture content, and 22.2% represents high moisture content sandy soil.

In terms of the soil parameters by the sinkage exponent n shown in Table 2, the table mainly includes the frictional modulus k_φ, the cohesive modulus k_c, the sinkage exponent n, the cohesion strength of the soil C, the soil adhesion strength Ca, the internal friction angle of the soil φ, the external friction angle of soil to steel δ and the soil density. the test soil had a relatively soft condition at each level of the moisture content. The cohesive strength and the adhesive strength had approximately equal values to each other at the respective level of the water content. Nevertheless, it could be found that the internal friction angle (soil-soil) was always greater than the external friction angle (soil-steel), and the difference between them was reduced with the increase in the water content of the soil.

TABLE 2. Experimental result of the soil parameters.

W. C. (%)	k_c (N/m^{n+1})	k_φ (N/m^{n+2})	n	C (kPa)	Int. friction angle (Degree)	Ca (kpa)	Ext. friction angle (Degree)	Density (kg/m^3)
1.4	5374.6	638006	0.861	0.1605	32.4	0.2761	18.48	1279
8.0	3661.8	105520	0.614	0.4202	16.5	1.0978	12.68	1087
14.7	173.2	154221	0.628	2.0715	15.71	2.1382	13.19	998
22.2	1668.2	340988	0.746	1.0281	19.27	1.1836	16.098	1625

FIGURE 6. Locale photo of the penetration device.

Prediction results of the shear forces

As mentioned above, the dimensions of the single grouser shoe remained unchanged except for the grouser height, which was changed from 0 cm to 15 cm with an interval of 0.5 cm. Every grouser shoe has been tested under four different moisture contents of the sandy loam. The forces acting on the grouser tip surface F_1, the two lateral surfaces F_2, and the bottom surface F_3 in the 3D direct shear model of the track-soil interaction system were predicted, respectively. The graphs for the relationship of F_1, F_2, and F_3 to the change of grouser heights were illustrated, as follows, in Figs. 7, 8, and 9, respectively.
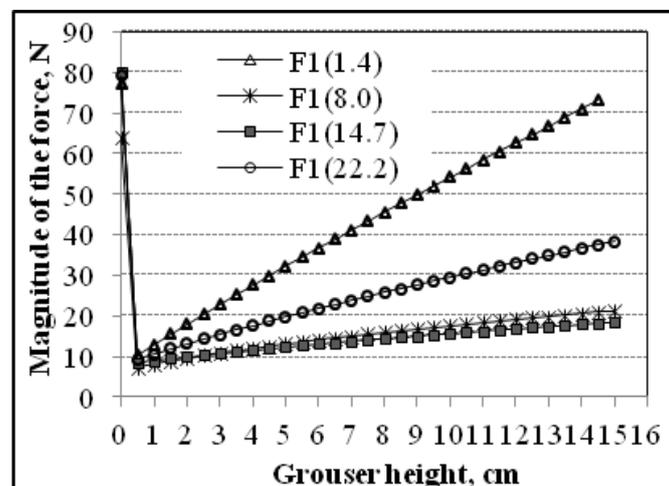
FIGURE 7. The Relationship of the F_1 changed with the increase of the grouser heights.

The horizontal force acting on the grouser tip surface was denoted by F_1. In Fig. 7, the four curves were the relationships of the F_1 to the grouser heights under four different moisture contents' soils. At each moisture content, the force F_1 had a linear relationship with the increase of the grouser height. Because the hardpan has not been considered under the topsoil, the linear relationship was kept even when the grouser height reached 15 cm. When the grouser height was 0 cm, the whole bottom surface of the single grouser shoe was considered the tip surface. Therefore, a greater value of F_1 was obtained at 0 cm grouser height based on Fig. 7. The smallest F_1 with the same single grouser shoe was at the moisture content of 14.7%, and the specific value was increased from 10 N to 20 N with the increase of the grouser height except for the 0 cm grouser height which has an extreme greater value at 80 N. The F_1 of tracks with different grouser heights under the soil of 8.0% moisture content were approximate to those with the soil condition under the 14.7% moisture content. In addition, the F_1 of the track with a grouser height at 0 cm under 8.0% moisture content soil has a value of approximately 65 N. For the soil moisture content of 22.2% and 1.4%, the F_1 of the track with 0 cm grouser were all at the value approximately 80 N. After that, both of them decreased to a value of approximately 10 N. From then on, both of them increased with the increase of the grouser height from 0.5 cm to 15 cm. However, the F_1 under the moisture content of 22.2% was changed from 10 N to 40 N, rather than those of 1.4% increased from 10 N to 75 N. According to Fig. 7, it could be known that the F_1 was increased with the increase of the grouser height under either moisture contents of the soil.

Lateral shear force F_2 consisted of the forces generated on two side surfaces in the 3D direct shear model. The relationship of F_2 with the increase of grouser height under different moisture contents soil has been graphed and shown in Fig. 8.

In the condition of four different moisture contents soil, the F_2 of the track with a grouser height of 0 cm all have low values less than 10 N according to Fig. 8. When the soil moisture content was 1.4%, at first, the F_2 increased from 0 to 21 N with the increase of the grouser height from 0 cm to 8 cm. From then on, the F_2 decreased from 21 N to 10 N with the increase of grouser height from 8 cm to 15 cm. A different trend could be found when the moisture contents were at 8.0%, 14.7%, and 22.2%. At those moisture content levels, the F_2 increased proportionally with the increase of the grouser height. Specifically, the increased range of 8.0% was from 3 N to 60 N, the increased range of 14.7% was from 10 N to 115 N, and the increased range of 22.2% was from 3 N to 67 N.
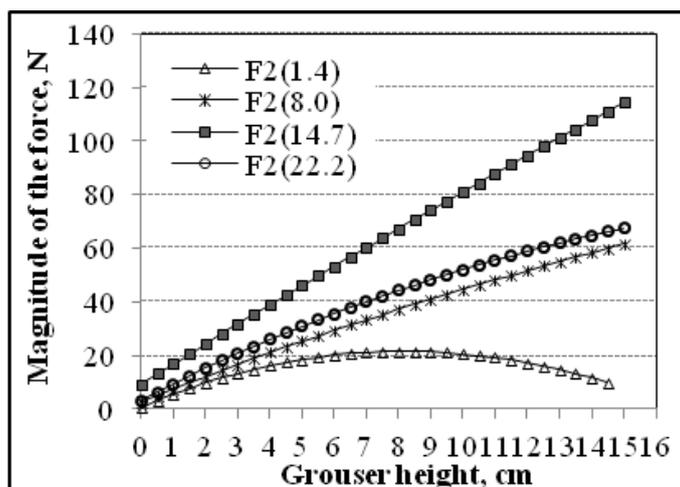
FIGURE 8. Relationship of the F_2 changed with the increase of the grouser heights.

On the horizontal direction of the track-soil interaction system, only the F_3 was generated just by a soil failure between soil-soil among F_1, F_2, and F_3. Fig. 9 illustrates how the F_3 changed with the changes in the grouser heights from 0 cm to 15 cm.

In Fig. 9, it could be known that F_3 has a more complicated relationship with each other than F_1 and F_2 when the soil moisture contents are at 1.4%, 8.0%, 14.7%, and 22.2%. When the grouser height was 0 cm, the F_3 were all equal to 0 N at either level of the moisture contents. The F_3 under the 1.4% moisture content soil got the largest force at the value of 123 N with a grouser height of 0.5 cm, and then it was rapidly decreased to 19 N with the increase of the grouser height to 15 cm. Comparing to the moisture content of 1.4%, the F_3 under the moisture content of other 3 levels decreased more gently. It was almost parallel to each other when the F_3 changed with the increase of the grouser height under the 8.0% and 14.7% moisture content soil. Furthermore, the F_3 of 8.0% moisture content decreased from 63 N to 50 N; meanwhile, the F_3 of 14.7% decreased from 80 N to 73 N with the increase of the grouser height. At the same time, the F_3 under the 22.2% moisture content soil was deceased from 80 N to 55 N with the increase of the grouser height from 0.5 cm to 15 cm.
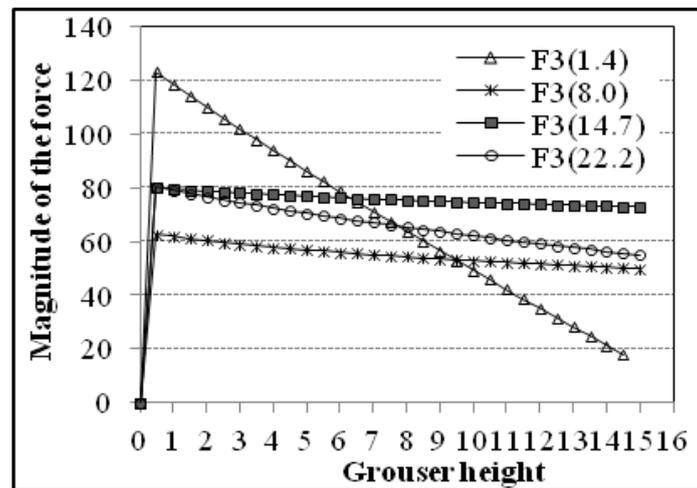
FIGURE 9. The relationship of the F_3 changed with the increase of the grouser heights.

Based on the above introductions for Figs. 7, 8, and 9, the shear forces F_1, F_2, and F_3 were influenced comprehensively by the soil conditions and the shape of the single grouser shoe. Because the internal friction was extremely large with an internal friction angle of 32.4°, a single grouser shoe with short grouser has a better performance on thrust generation when the soil moisture content was 1.4%. Subsequently, the soil's volume increased with the moisture content increased to 8.0%, which means the soil has a loose texture and low values of cohesion strength, adhesion strength, and friction. In this kind of soil condition, a grouser shoe with a long grouser was recommended. As the moisture content increased to 14.7% and 22.2%, the soil's cohesion and adhesion strength rapidly increased; simultaneously, the friction of the soil almost kept no changes. Consequently, a moderate grouser height, such as 6 or 7 cm, was better for generating the drawbar pull of the track.

CONCLUSIONS

In this study, one kind of sandy loam and a single grouser shoe have been utilized for predicting the horizontal shear forces on the grouser tip surface, the two side surfaces, and the bottom surface in the 3D direct shear model. Based on the experimental results and the discusses, it could be concluded as follows:

(1) For the sandy loam condition, the force F_3, which was acting on the bottom surface, was greater than the shear force on two lateral surfaces F_2. Simultaneously, the F_1, which was acting on the tip surface, had the smallest contribution to the drawbar pull of the track-soil interaction system.

(2) In an extremely dry sandy loam condition, such as 1.4% moisture content, the track should be equipped with grouser shoes with short or even no grouser.

(3) Depending on different soil moisture contents, the study on the shear forces acting on different surfaces of the track-soil interaction system was significant for optimizing the dimensions of the grouser shoe.

REFERENCES

Ani OA, Uzoejinwa BB, Ezeama AO, Onwualu AP, Ugwu SN, Ohagwu CJ (2018) Overview of soil-machine interaction studies in soil bins. Soil and Tillage Research 175: 13-27.

Baek S, Shin G, Chung C (2018) Assessment of the side thrust foroff-road tracked vehicles based on the punching shear theory. Journal of Terramechanics 79: 59-68.

Battiato A, Diserens E (2017) Tractor traction performance simulation on differently textured soils and validation: a basic study to make traction and energy requirements accessible to the practice. Soil and Tillage Research 166: 18-32.

Bekker MG (1956) The Theory of Land Locomotion. Ann Arbor: University of Michigan Press.

Bekker MG (1969) Introduction to terrain-vehicle systems. Ann Arbor, The University of Michigan Press.

Cutini M, Brambilla M, Toscano P, Bisaglia C, Abbati G, Meloro G (2020) Evaluation of drawbar performance of winter tyres for special purpose vehicles. Journal of Terramechanics 87: 29-36.

Das BM (1979) Introduction to soil mechanics. AMES, The Iowa State University Press.

Edwin P, Shankar K, Kannan K (2018) Soft soil track interaction modeling in single rigid body tracked vehicle models. Journal of Terramechanics 77: 1-14.

Feng XU, Qiu-hua RAO, Wen-bo MA (2018) Turning traction force of tracked mining vehicle based on rheological property of deep-sea sediment. Transactions of Nonferrous Metals Society of China 28(6): 1233-1240.

Ge J, Wang X, Kito K (2016a) Comparing tractive performance of steel and rubber single grouser shoe under different soil moisture contents. International Journal of Agricultural & Biological Engineering 9(2): 11-20.

Ge J, Wang X, Kito K (2016b) Effect of soil adhesion on tractive performance of single grouser. International Agricultural Engineering Journal 25(1): 20-29.

Ge J, Zhang D, Wang X, Cao C, Fang L, Duan Y (2019) Tractive performances of single grouser shoe affected by different soils with varied moisture contents. Advances in Mechanical Engineering 11(5):1687814019849133.

Gill WR, Vanden Berg GE (1967) Soil dynamics in tillage and traction. Washington: Government Printing Office. (Agricultural Handbook, 316).

Guo T, Guo J, Huang B, Peng H (2019) Power consumption of tracked and wheeled small mobile robots on deformable terrains–model and experimental validation. Mechanism and Machine Theory 133: 347-364.

Li Y, He D, Si Q, Meng X (2021) Effect of track shoes structural parameters on traction performance of unmanned underwater tracked bulldozer. Ocean Engineering 237: 109655.

Lyasko M (2010) Multi-pass effect on off-road vehicle tractive performance. Journal of Terramechanics 47(5): 275-294.

Mason GL, Salmon JE, McLeod S, Jayakumar P, Cole MP, Smith W (2020) An overview of methods to convert cone index to bevameter parameters. Journal of Terramechanics 87: 1-9.

Mocera F, Nicolini A (2018) Multibody simulation of a small size farming tracked vehicle. Procedia Structural Integrity 8: 118-125.

Nassiraei AAF, Skonieczny K (2020) Grousers improve drawbar pull by reducing resistance and generating thrust at the front of a wheel. Journal of Terramechanics 91: 73-84.

Plackett CW (1985) A review of force prediction methods for off-road wheels. Journal of Agricultural Engineering Research 31(1): 1-29.

Sandu C, Taheri Sh, Taheri S, Gorsich D (2019) Hybrid Soft Soil Tire Model (HSSTM). Part II: Tire-terrain interaction Journal of Terramechanics 86: 15-29.

Shaikh SA, Li Y, Ma Z, Chandio FA, Tunio MH, Liang Z,Solangi KA (2021) Discrete element method (DEM) simulation of single grouser shoe-soil interaction at varied moisture contents. Computers and Electronics in Agriculture 191: 106538.

Shin G-B, Baek S-H, Park K-H, Chung C-K (2020) Investigation of the soil thrust interference effect for tracked unmanned ground vehicles (UGVs) using model track tests. Journal of Terramechanics 91: 117-127.

Suzuki H, Katsushima K, Ozaki S (2019) Study on applicability of RFT to traveling analysis of wheel with grousers: comparison with DEM analysis as a virtual test. Journal of Terramechanics 83: 15-24.

ten Damme L, Schjønning P, Munkholm LJ, Green O, Nielsen SK, Lamandé M (2021) Soil structure response to field traffic: Effects of traction and repeated wheeling. Soil and Tillage Research 213:105128.

Tiwari VK, Pandey KP, Pranav PK (2010) A review on traction prediction equations. Journal of Terramechanics 47(3): 191-199.

Wang W, Yan Z, Du Z (2018) Experimental study of a tracked mobile robot's mobility performance. Journal of Terramechanics 77: 75-84.

Wong JY (2008) Theory of ground vehicles. New Jersey, John Wiley.

Wong JY (2010) Terramechanics and Off-Road Vehicle Engineering. Elsevier, Oxford, England.

Wong JY, Jayakumar P, Toma E, Preston-Thomas J (2018) Comparison of simulation models NRMM and NTVPM for assessing military tracked vehicle cross-country performance. Journal of Terramechanics 80: 31-48.

Xu Z, Liu Y, Yang G, Xia J, Dou Z, Meng Q, Xu X (2022) Research on contact model of track-soft sediment and traction performance of four-tracked seabed mining vehicle. Ocean Engineering 259: 111902.

Yamada M, Yamauchi G, Hashimoto T (2021) Fundamental study on underwater trafficability for tracked vehicle. Journal of Terramechanics 98: 42-49.

Yang C, Yang G, Liu Z, Chen H, Zhao Y (2018) A method for deducing pressure–sinkage of tracked vehicle in rough terrain considering moisture and sinkage speed. Journal of Terramechanics 79: 99-113.

Yokoyama A, Nakashima H, Shimizu H, Miyasaka J, Ohdoi K (2020) Effect of open spaces between grousers on the gross traction of a track shoe for lightweight vehicles analyzed using 2D DEM. Journal of Terramechanics 90: 31-40.

Yuta S (2017) Development of a remotely controlled semi-underwater heavy carrier robot for unmanned construction works. Journal of Disaster Research 12(3): 432-445.

Zhang J, Shi D, Jin H, Li H, Jiang N, Ye Q (2022) Characteristics of cultivated layer soil shear strength for sloping farmland in response to soil erosion in the Three Gorges Reservoir Area. CATENA 215: 106304.

Zhou L, Gao J, Hu C, Li Q (2021) Numerical simulation and testing verification of the interaction between track and sandy ground based on discrete element method. Journal of Terramechanics 95: 73-88.